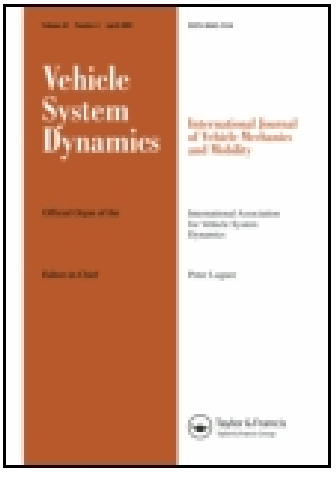

Vehicle System Dynamics: International Journal of Vehicle Mechanics and Mobility

Publication details, including instructions for authors and subscription information:
http://www.tandfonline.com/loi/nvsd20

An improved Magic Formula/Swift tyre model that can handle inflation pressure changes

I. J.M. Besselink [a], A. J.C. Schmeitz [b] & H. B. Pacejka [c]

[a] Department of Mechanical Engineering, Eindhoven University of Technology, P.O. Box 513, 5600 MB, Eindhoven, The Netherlands

[b] TNO Automotive, Helmond, The Netherlands

[c] TU Delft, Delft, The Netherlands

Published online: 26 Nov 2010.

To cite this article: I. J.M. Besselink, A. J.C. Schmeitz & H. B. Pacejka (2010) An improved Magic Formula/Swift tyre model that can handle inflation pressure changes, Vehicle System Dynamics: International Journal of Vehicle Mechanics and Mobility, 48:S1, 337-352, DOI: 10.1080/00423111003748088

To link to this article: http://dx.doi.org/10.1080/00423111003748088

Vehicle System Dynamics
Vol. 48, Supplement, 2010, 337–352

Taylor & Francis
Taylor & Francis Group

An improved Magic Formula/Swift tyre model that can handle inflation pressure changes

I.J.M. Besselink[a]*, A.J.C. Schmeitz[b] and H.B. Pacejka[c]

[a] *Department of Mechanical Engineering, Eindhoven University of Technology, P.O. Box 513, 5600 MB Eindhoven, The Netherlands;* [b] *TNO Automotive, Helmond, The Netherlands;* [c] *TU Delft, Delft, The Netherlands*

(*Received 19 October 2009; final version received 3 March 2010*)

This paper describes extensions to the widely used TNO MF-Tyre 5.2 Magic Formula tyre model. The Magic Formula itself has been adapted to cope with large camber angles and inflation pressure changes. In addition, the description of the rolling resistance has been improved. Modelling of the tyre dynamics has been changed to allow a seamless and consistent switch from simple first-order relaxation behaviour to rigid ring dynamics. Finally, the effect of inflation pressure on the loaded radius and the tyre enveloping properties is discussed and some results are given to illustrate the capabilities of the model.

Keywords: simulation; tyre dynamics models; tyre dynamics measurement; tyre dynamics; Magic Formula

1. Introduction

Since its conception over 20 years ago, the Magic Formula has fairly quickly been adopted as the industry standard tyre model for vehicle handling simulations. Over the years various developments have been made to improve the accuracy and to extend the capabilities of the model, for example, the method to describe combined slip has been improved and a special Magic Formula has been developed to handle the large camber angles occurring on motorcycles. In parallel, research has been done to increase the frequency range by introducing rigid ring dynamics, contact patch transients and an obstacle enveloping model, also known as the SWIFT or MF-Swift model. An overview and description of these developments can be found in Pacejka [1].

The fact that from the start the tyre model equations were published in the open literature has certainly contributed to the popularity of the Magic Formula. On the other hand, over the years it has also resulted in a number of different, at times incompatible, implementations. Different versions of the Magic Formula may be used, equations are sometimes partially implemented, in-house extensions are added, different axis system or units are used, etc.

*Corresponding author. Email: i.j.m.besselink@tue.nl

ISSN 0042-3114 print/ISSN 1744-5159 online

DOI: 10.1080/00423111003748088
http://www.informaworld.com

Notwithstanding these issues, the TNO MF-Tyre 5.2 tyre model has reached a mature status and is widely used in the industry for vehicle handling studies. The model equations are documented in TNO [2].

To move forward from MF-Tyre 5.2, several targets have been defined:

- To improve the description of camber, that is, to have an explicit formulation and control over the camber stiffness and to extend the capabilities of the model for handling very large camber angles. This will make the special 'motorcycle' Magic Formula superfluous and improves processing of measurements according to the TIME procedure.
- To include the effect of inflation pressure changes in the Magic Formula. This will eliminate the need to have separate parameter sets (tyre property files) for different tyre pressures. It will allow evaluating tyre behaviour for pressures not in the measurement programme and it also leads to a reduction in the total number of measurements required.
- To make the description of tyre dynamics consistent between MF-Swift and MF-Tyre. For example, when including the dynamics of the tyre belt, the path-dependent (basic) tyre relaxation behaviour should remain unchanged.

In addition, various other enhancements have been made, for example, in the description of rolling resistance and overturning moment. This paper aims to introduce the MF-Tyre/MF-Swift 6.1 model and accompanying equations. Due to space restrictions and the extent of the changes that were made in comparison with the MF-Tyre 5.2 model, turn slip extensions [1] will not be discussed.

2. Contact point, loaded radius and calculation of slip

Traditionally, the tyre force and moment characteristics are defined in the tyre road contact point. The location of this point is defined by considering the tyre/wheel combination as an infinitely thin disk through the plane of symmetry of the tyre, as is shown in Figure 1.

It is important to note that in practice the forces and moments are not measured at the tyre road contact point C, but at the wheel centre. In order to process the measurements and to calculate the forces and moments at the ground contact point, both the height of the wheel centre and inclination angle γ are required. Consequently, the distance from wheel centre to ground contact point, that is, the loaded radius R_l, should be represented accurately in the tyre simulation model.

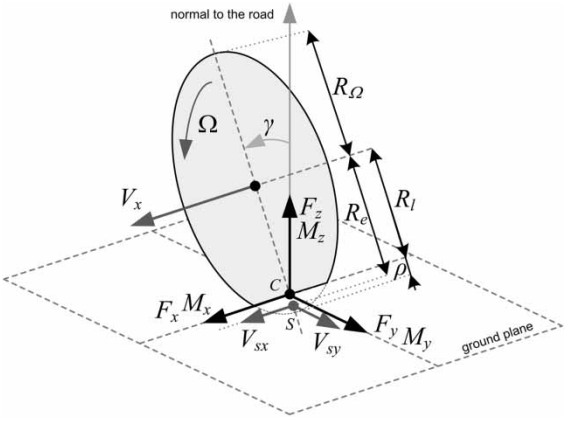

Figure 1. Force, moment and kinematic variables of the tyre road contact (ISO sign convention).

First, centrifugal growth of the free tyre radius R_Ω is calculated using the following formula:

$$R_\Omega = R_0 \left(q_{\mathrm{re0}} + q_{\mathrm{v1}} \left(\frac{\Omega R_0}{V_0} \right)^2 \right), \tag{1}$$

where R_0 equals the non-rolling free tyre radius, V_0 a reference velocity, Ω the wheel rotational velocity and q_{re0} and q_{v1} the model parameters. The tyre deflection ρ is the difference between the free tyre radius R_Ω and the loaded tyre radius R_l:

$$\rho = \max(R_\Omega - R_\mathrm{l}, 0). \tag{2}$$

The vertical tyre force F_z is then calculated using the following formula:

$$F_z = \left(1 + q_{\mathrm{v2}} \frac{R_0}{V_0} |\Omega| - \left(\frac{q_{Fcx} F_x}{F_{z0}} \right)^2 - \left(\frac{q_{Fcy} F_y}{F_{z0}} \right)^2 \right) \left(q_{Fz1} \frac{\rho}{R_0} + q_{Fz2} \left(\frac{\rho}{R_0} \right)^2 \right) \cdot (1 + p_{Fz1}\, \mathrm{dp}_i) F_{z0}. \tag{3}$$

Various effects are included in this calculation: a stiffness increase with velocity (q_{v2}), vertical sinking due to longitudinal and lateral forces (q_{Fcx}, q_{Fcy}), a quadratic force deflection characteristic (q_{Fz1}, q_{Fz2}) and the influence of the tyre inflation pressure (p_{Fz1}). Further, F_{z0} is the nominal load and dp_i the non-dimensional pressure increment, see appendix. For large camber angles (e.g. motorcycle tyres), a modified approach for calculating the vertical force is necessary, taking into account the contour of the tyre. Its discussion is outside the scope of this paper.

The vertical stiffness c_{z0} at the nominal vertical load, nominal inflation pressure, no tangential forces and zero forward velocity can be calculated as follows:

$$c_{z0} = \frac{F_{z0}}{R_0} \sqrt{q_{Fz1}^2 + 4 q_{Fz2}}. \tag{4}$$

In the expressions for the effective rolling radius and contact patch dimensions, the vertical stiffness adapted for tyre inflation pressure is used:

$$c_z = c_{z0}(1 + p_{Fz1}\, \mathrm{dp}_i). \tag{5}$$

The forces (F_x, F_y) and moments (M_x, M_y, M_z) at the ground contact point are functions of vertical force F_z, various slip properties, inclination angle γ, forward velocity V_x and inflation pressure p_i. These nonlinear relations are captured in the Magic Formula. The longitudinal slip is defined as the ratio of the longitudinal slip velocity V_{sx} and forward velocity V_x:

$$\kappa = -\frac{V_{sx}}{V_x} = -\frac{V_x - \Omega R_\mathrm{e}}{V_x} = -\frac{\Omega_\mathrm{fr} - \Omega}{\Omega_\mathrm{fr}} = \frac{\Omega}{\Omega_\mathrm{fr}} - 1. \tag{6}$$

In this equation, Ω_fr is the angular velocity of the freely rolling tyre. When executing measurements the latter part of this equation may be used to determine the amount of longitudinal slip. In the tyre simulation model, the first part of the equation is used, requiring an explicit equation for the effective rolling radius R_e. The ratio of the forward velocity of the wheel centre V_x to the angular velocity of the free rolling tyre Ω_fr equals the effective rolling radius R_e. The following empirical formula is used:

$$R_\mathrm{e} = R_\Omega - \frac{F_{z0}}{c_z} \left(D_{\mathrm{reff}} \arctan \left(B_{\mathrm{reff}} \frac{F_z}{F_{z0}} \right) + F_{\mathrm{reff}} \frac{F_z}{F_{z0}} \right), \tag{7}$$

where D_{reff}, B_{reff} and F_{reff} are model parameters. When no measurements are available, the suggested values are $D_{\mathrm{reff}} = 0.24$, $B_{\mathrm{reff}} = 8$ and $F_{\mathrm{reff}} = 0.01$. The effective rolling radius

defines the slip point S. Note that the location of S is different from the contact point C as is shown in Figure 1. Point S is also used to calculate the sideslip angle α using the lateral slip velocity V_{sy}:

$$\alpha = \arctan\left(\frac{V_{sy}}{V_x}\right). \tag{8}$$

It is clear that in order to get an accurate representation of the tyre characteristics consistent definitions for slip should be used. Though one can argue on the exact definition of slip variables, it is clear that in any case consistent definitions should be used for both the measurements and the simulation model. The definitions given in this section have been used since 1996 in the various MF-Tyre simulation models (including MF-Tyre 5.2). When modelling the tyre-road enveloping and relaxation behaviour the dimensions of the tyre contact patch are needed. The empirical expressions for half of the contact length a and half of the width b read as follows:

$$a = R_0\left(q_{ra2}\frac{F_z}{c_z R_0} + q_{ra1}\sqrt{\frac{F_z}{c_z R_0}}\right) \approx R_0\left(q_{ra2}\frac{\rho}{R_0} + q_{ra1}\sqrt{\frac{\rho}{R_0}}\right), \tag{9}$$

$$b = w\left(q_{rb2}\frac{F_z}{c_z R_0} + q_{rb1}\left(\frac{F_z}{c_z R_0}\right)^{1/3}\right) \approx w\left(q_{rb2}\frac{\rho}{R_0} + q_{rb1}\left(\frac{\rho}{R_0}\right)^{1/3}\right), \tag{10}$$

where w is the nominal width of the tyre. Since these expressions are functions of the tyre deflection ρ, the effect of changing the tyre inflation pressure is taken into account. Lowering the inflation pressure results in an increase in tyre deflection and thus an increase in contact length.

3. Steady-state force and moment characteristics

For an introduction to Magic Formula tyre modelling, we refer to Pacejka [1, pp. 172–184]. Initially, the Magic Formula has been designed to describe the force and moment characteristics of passenger car tyres within a limited camber range ($\pm 15°$). Beyond this range extrapolation errors may occur and as such the formula proved not to be suitable for describing tyre characteristics at large inclination angles. This resulted in a different Magic Formula equation for motorcycle tyres, as proposed by De Vries [3], where the contributions of camber and sideslip are fully separated, as is shown in Equation (11):

$$F_y = D_y \sin\begin{pmatrix} C_y \arctan((1-E_y)B_y\alpha_y + E_y \arctan(B_y\alpha_y)) \\ +\, C_\gamma \arctan((1-E_\gamma)B_\gamma\gamma + E_\gamma \arctan(B_\gamma\gamma)) \end{pmatrix}. \tag{11}$$

This approach was subsequently adopted in a slightly modified form for the MF–MC Tyre model, aimed specifically at motorcycle tyres. This model is described in Pacejka [1, pp. 579–583]. One of the benefits of this approach is that the camber stiffness is defined explicitly, which also proves to be convenient when new approaches to tyre measurements, like the TIME procedure [4], are used. A logical step would be to also use the MF-MC Tyre model for passenger car tyres, but the accuracy proved to be less compared with the normal Magic Formula. An attempt was made to adapt the MF–MC Tyre model to suit passenger car tyre characteristics better, but this model, also known as MF-Time [5], still suffers from a reduced accuracy with respect to the normal Magic Formula for passenger car tyres.

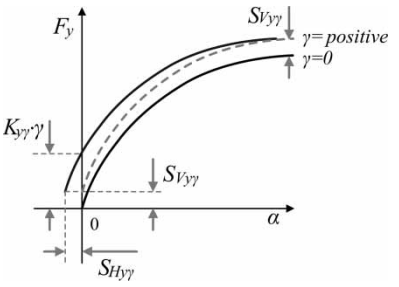

Figure 2. Creating the side force characteristic at an inclination angle by applying vertical and horizontal shifts.

It turns out that only limited modifications to the MF-Tyre 5.2 equations are required to overcome these issues. First, the vertical shift in the lateral force $S_{Vy\gamma}$ due to camber (and vertical force) remains the same:

$$S_{Vy\gamma} = F_z(p_{Vy3} + p_{Vy4}\,\mathrm{df}_z)\gamma, \tag{12}$$

where df_z is the dimensionless load increment and p_{Vy3} and p_{Vy4} are some model parameters, see appendix. The camber stiffness $K_{y\gamma}$ is specified in exactly the same way as in the MF–MC Tyre model:

$$K_{y\gamma} = (p_{Ky6} + p_{Ky7}\,\mathrm{df}_z)F_z. \tag{13}$$

Now the required horizontal shift (or sideslip angle) due to camber can be calculated using the cornering stiffness $K_{y\alpha}$:

$$S_{Hy\gamma} = \frac{K_{y\gamma}\gamma - S_{Vy\gamma}}{K_{y\alpha}}. \tag{14}$$

This approach is illustrated in Figure 2. The side force characteristic is shifted vertically by a magnitude $S_{Vy\gamma}$ to account for the increase in side force due to an inclination angle for large values of side slip. At zero side slip angle, we demand that the side force due to an inclination of the tyre equals $K_{y\gamma}\gamma$. Since the slope of F_y versus α curve is known, it is equal to the cornering stiffness $K_{y\alpha}$, the magnitude of the required horizontal shift can be easily calculated using Equation (14). In this simplified explanation, we ignore initial offsets for zero inclination angle and changes of the shape of F_y versus α curve due to an inclination angle.

It appears that this straightforward modification enables to use a single Magic Formula for large camber angles, without making sacrifices with respect to accuracy for normal passenger car tyres. The modifications to the expressions for the self-aligning moment M_z are also fairly limited. The main changes being an extended expression for the peak value of the residual moment M_{zr} [D_r, Equation (A64)] and the fact that the side force at zero camber is used in the expression for the self-aligning moment [Equation (A49)], which is similar to MF–MC Tyre. Figure 3 illustrates the capabilities of this modified Magic Formula for representing the measured characteristics of a motorcycle tyre. The new equations have also been tested on a large database with force and moment measurements, consisting of 55 passenger car tyres, 14 motorcycle tyres, 27 racing tyres and 10 truck tyres. The fitting errors, representing the difference between measurements and model, are presented in Table 1.

The following conclusions can be draw from Table 1:

- For normal tyres the difference between MF-Tyre 5.2 and MF-Tyre 6.1 is negligible and the accuracy is approximately the same.

- The MF-Time model is less accurate in comparison with the MF-Tyre 5.2, in particular the representation of the self-aligning moment appears to be worse.
- MF-Tyre 6.1 can represent motorcycle tyre behaviour quite accurately: the fitting error of the side force characteristic is even reduced in comparison with the MF–MC Tyre, though the self-aligning moment is somewhat less accurate.

So a single set of Magic Formula equations has been developed which can represent passenger car, truck, racing and motorcycle tyres with a similar accuracy as obtained with different magic formula tyre models used by the industry today. The MF-Tyre 6.1 equations have the advantage of including an explicit formulation of the camber stiffness and they can cope with large camber angles. Next, the expressions have been extended to include the effect of tyre inflation pressure changes on the tyre force and moment characteristics.

It is clear that for many passenger cars on the road the same tyres are used on the front and rear axle, but the tyre pressure is different and may need to be adjusted for different vehicle loading conditions. The Magic Formula equations published to date do not account for tyre pressure changes, leading to multiple parameter datasets for different tyre pressures and an additional measurement effort. Furthermore, only the inflation pressures tested can be selected and it is not possible to perform an interpolation.

As the Magic Formula is a semi-empirical tyre model, each individual tyre characteristic has to be analysed for the impact of changes to the tyre inflation pressure [6,7]. Both measurements

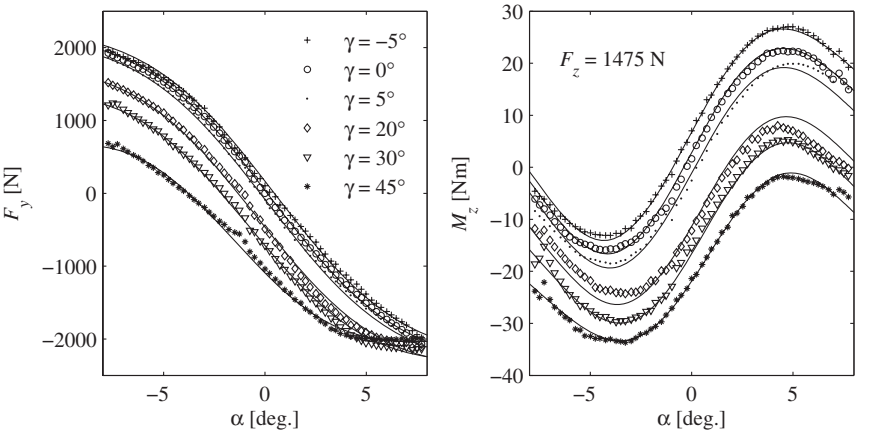

Figure 3. MF-Tyre 6.1 fit of a motorcycle tyre, left: side force, right: self-aligning moment; markers are measurements (source: TNO Tyre Test Trailer) and continuous lines are Magic Formula results.

Table 1. Comparison of average fitting errors for various tyre models and different tyre types.

	Car/truck/race tyres ($n = 92$)			Motorcycle tyres ($n = 14$)	
Force/slip case	MF-Tyre 5.2	MF-Time	MF-Tyre 6.1	MF−MC Tyre 1.1	MF-Tyre 6.1
F_x pure (%)	4.17	4.16	4.17	4.11	4.06
F_y pure (%)	2.37	2.73	2.26	4.55	4.28
M_z pure (%)	6.47	9.53	6.23	8.76	10.19
F_x combined (%)	5.70	5.69	5.70	4.46	4.43
F_y combined (%)	8.58	8.81	8.53	11.06	11.01
M_z combined (%)	32.74	34.57	32.49	40.59	40.29

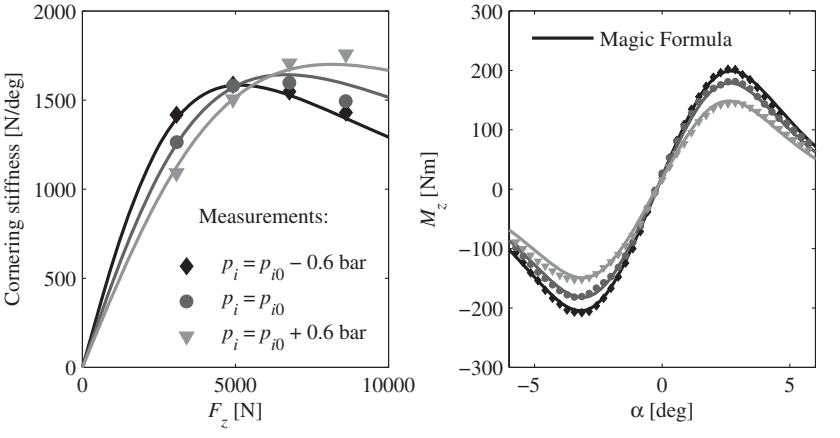

Figure 4. Tyre pressure effects for a passenger car tyre; left: cornering stiffness and right: self-aligning moment.

and a physical background model were used in this process. The main effects identified are as follows:

- changes in longitudinal slip stiffness, cornering stiffness and camber stiffness;
- changes in peak friction coefficient, both longitudinal and lateral;
- a reduction of the pneumatic trail with increasing inflation pressure.

Details on the modified equations can be found in the appendix. As an example, the cornering stiffness and self-aligning moment characteristics are shown in Figure 4. Since the effect of tyre inflation pressure on, for example, the combined slip characteristics is small, it is sufficient to measure this behaviour at a single inflation pressure and the total number of tests can therefore be reduced. Details on the testing requirements can be found in the TNO tyre model documentation [8].

As energy efficiency of road vehicles is becoming even more important, an accurate modelling of the rolling resistance of the tyres should be addressed. In the SWIFT model the increase in rolling resistance at high forward velocities has already been identified. Next, the nonlinear dependency on the vertical force and inflation pressure has been added.

In Michelin [9], the following equation is given to adapt the rolling resistance for conditions deviating from the ISO rolling resistance test:

$$f_{\mathrm{rr}} = f_{\mathrm{rr,ISO}} \left(\frac{p_i}{p_{i,\mathrm{ISO}}} \right)^{\alpha} \left(\frac{F_z}{F_{z,\mathrm{ISO}}} \right)^{\beta}, \tag{15}$$

where f_{rr} is the rolling resistance coefficient, p_i the tyre inflation pressure and F_z the vertical tyre force. According to Michelin [9], the following coefficients are applicable: $\alpha = -0.4$ and $\beta = 0.85$ for a passenger car and $\alpha = -0.2$ and $\beta = 0.9$ for a truck tyre. This equation has been adopted in a slightly modified form and has been combined with the existing velocity influence and reads (not including the camber effects) for the rolling resistance moment as follows:

$$M_y = -R_0 F_{z0} \lambda_{My} \left(q_{sy1} + q_{sy2} \frac{F_x}{F_{z0}} + q_{sy3} \left| \frac{V_x}{V_0} \right| + q_{sy4} \left(\frac{V_x}{V_0} \right)^4 \right) \left(\frac{F_z}{F_{z0}} \right)^{q_{sy7}} \left(\frac{p_i}{p_{i0}} \right)^{q_{sy8}}. \tag{16}$$

Figure 5 shows that following this approach the rolling resistance can be modelled accurately for a standard passenger car tyre.

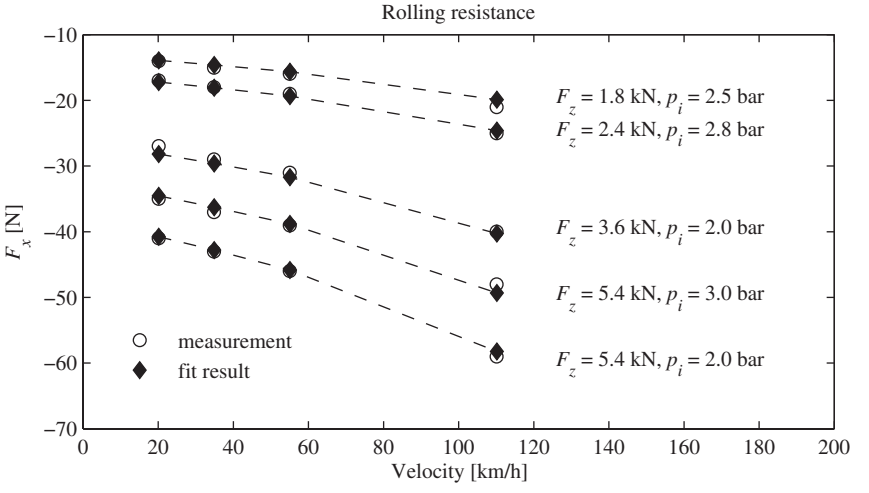

Figure 5. Rolling resistance force as a function of vertical force, inflation pressure and forward velocity.

4. Tyre relaxation behaviour and belt dynamics

In the MF-Tyre 5.2 tyre model, an empirical relation is used to describe the relaxation length dependency on vertical force. In the SWIFT model, the dynamics are modelled using a rigid ring approach, residual stiffness and contact patch relaxation model. Ultimately, these two different approaches could potentially result in simulating a different relaxation length for the same tyre, which obviously is not acceptable. Depending on the application there will be a need to be able to switch the model from a simple representation of the dynamics to a more elaborate but more time consuming variant. Furthermore, the inflation pressure is considered in the model, which also has an impact on the relaxation behaviour.

The solution for this combined set of requirements is to model the overall longitudinal and lateral tyre stiffness and calculate the required parameters from these expressions. The following expressions are used to describe the overall longitudinal c_x and lateral stiffness c_y of the tyre at ground contact:

$$c_x = c_{x0}\left(1 + p_{cfx1}\,\mathrm{df}_z + p_{cfx2}\,\mathrm{df}_z^2\right)\left(1 + p_{cfx3}\,\mathrm{dp}_i\right), \tag{17}$$

$$c_y = c_{y0}\left(1 + p_{cfy1}\,\mathrm{df}_z + p_{cfy2}\,\mathrm{df}_z^2\right)\left(1 + p_{cfy3}\,\mathrm{dp}_i\right), \tag{18}$$

where c_{x0} and c_{y0} are the longitudinal and lateral stiffness of the tyre at the nominal vertical force and inflation pressure. Using these stiffness and the longitudinal slip stiffness $K_{x\kappa}$ and cornering stiffness $K_{y\alpha}$, the relaxation lengths for longitudinal and sideslip are, respectively,

$$\sigma_x = \frac{K_{x\kappa}}{c_x}, \tag{19}$$

$$\sigma_y = \frac{K_{y\alpha}}{c_y}. \tag{20}$$

In principle, the stiffness c_x and c_y could be measured on a non-rolling tyre, but the preferred approach is to measure the cornering stiffness and lateral relaxation length in a transient test for a number of different inflation pressures and vertical loads. Subsequently, the lateral stiffness equation can be fitted to these measurement points accordingly. Figure 6 gives an impression of

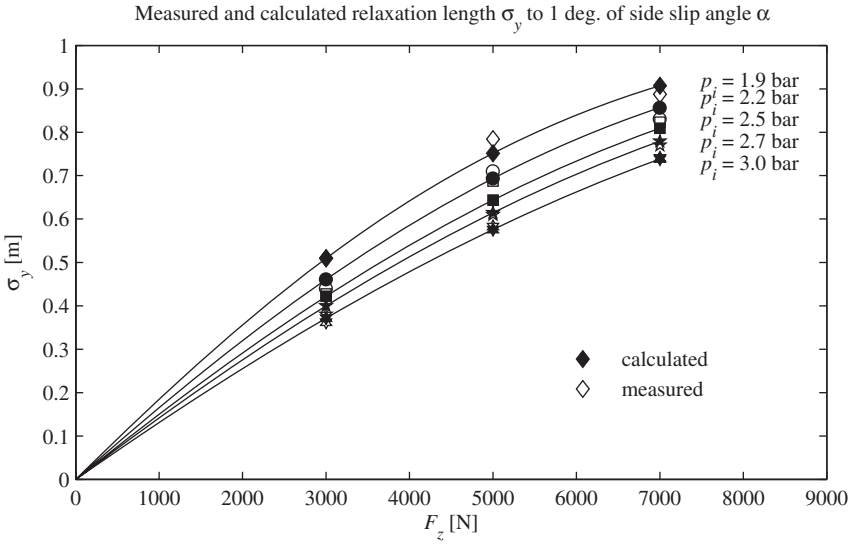

Figure 6. Lateral relaxation length as a function of vertical force and inflation pressure.

the dependency of the lateral relaxation length on the vertical force and tyre inflation pressure for a standard passenger car tyre.

Next to the steady-state representation, three approaches with increasing complexity are possible to model the tyre transient behaviour and dynamics.

4.1. *Linear transients*

The relaxation length is determined using Equations (19) and (20) and is subsequently used in the next two differential equations to calculate the (transient) slip quantities:

$$\sigma_x \dot{\kappa} = -V_x \kappa - V_{sx}, \tag{21}$$

$$\sigma_y \dot{\alpha} = -V_x \alpha + V_{sy}. \tag{22}$$

4.2. *Nonlinear transients*

In this approach, the tyre-road contact is separated into two parts and can be considered as a series connection of a spring-damper with a relaxation system (Figure 7):

$$k_{cy} \dot{\varepsilon}_y + c_{cy} \varepsilon_y = F_y, \tag{23}$$

$$\sigma_c \dot{\alpha} = -V_x \alpha + V_{sy} + \dot{\varepsilon}_y, \tag{24}$$

where σ_c equals half of the contact length a and ε_y is the lateral carcass deflection. The carcass stiffness c_{cy} is calculated as follows:

$$c_{cy} = \frac{K_{y\alpha}}{K_{y\alpha} - c_y a} c_y. \tag{25}$$

The same method can be used in the longitudinal direction. The benefit of this approach is the resulting decreasing relaxation behaviour with increasing sideslip angle. Also, the relaxation behaviour of the tyre on changes in vertical force is more accurately captured in this approach.

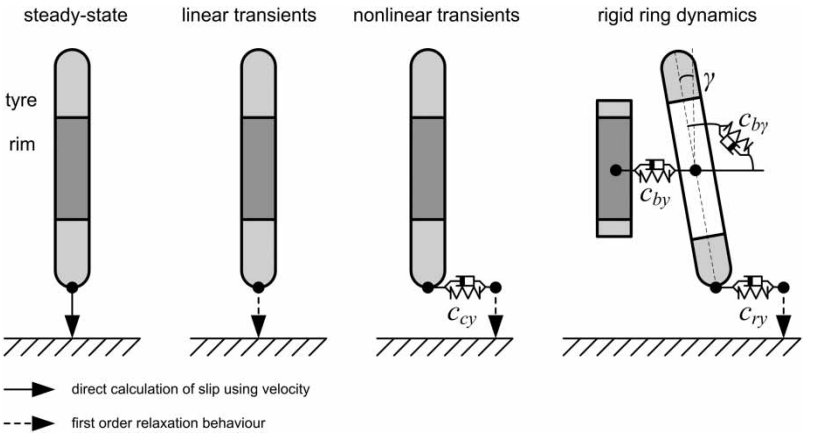

Figure 7. Schematic overview of different ways to model the contact transients/dynamics.

4.3. *Rigid ring dynamics*

When including rigid ring dynamics, the spring-damper system is now subdivided into various components as shown in Figure 7. In this case, the eigenfrequencies of the tyre belt determine the stiffness between rim and belt; still the overall stiffness is specified by Equations (17) and (18). This implies, for example, that the residual stiffness c_{ry} is calculated from

$$\frac{1}{c_y} = \underbrace{\frac{1}{c_{by}} + \frac{R_\mathrm{l}^2}{c_{b\gamma}} + \frac{1}{c_{ry}}}_{\text{carcass}} + \underbrace{\frac{a}{K_{y\alpha}}}_{\text{contact patch}} \quad , \tag{26}$$

in which c_{by} and $c_{b\gamma}$ are the lateral stiffness and rotational stiffness about the longitudinal axis between belt and rim. As is to be expected, the eigenfrequencies of the tyre belt will be higher when the tyre inflation pressure is increased. Empirical relations have been developed to account for this effect using a physical background model [7]. Some other aspects have to be taken into account, but are not discussed here due to space limitations:

- correction of the tyre sideslip angle for the twist of the contact patch;
- the transient dynamics of the self-aligning moment;
- combining the radial belt stiffness with the loaded radius equation.

5. Enveloping behaviour

To describe the tyre behaviour accurately on road unevenness with short wavelengths an enveloping model using elliptical cams has been developed by Schmeitz [10]. Research has shown that the shape of the elliptical cams does not change with tyre inflation pressure and that the tyre stiffness and contact length change cause the main effect [6]. Figure 8 shows the results of a low speed enveloping test with fixed axle height and initial vertical force of 4000 N. As the tyre pressure is increased, the stiffness increases and the contact length becomes smaller, resulting in larger forces and a shorter response. This is represented quite accurately by the model. The results for a high speed cleat test are shown in Figure 9. This figure clearly shows different responses for different inflation pressure: with increasing inflation pressure the frequency of the vertical mode increases, the peak loads increase and the excitation level of the vertical mode reduces.

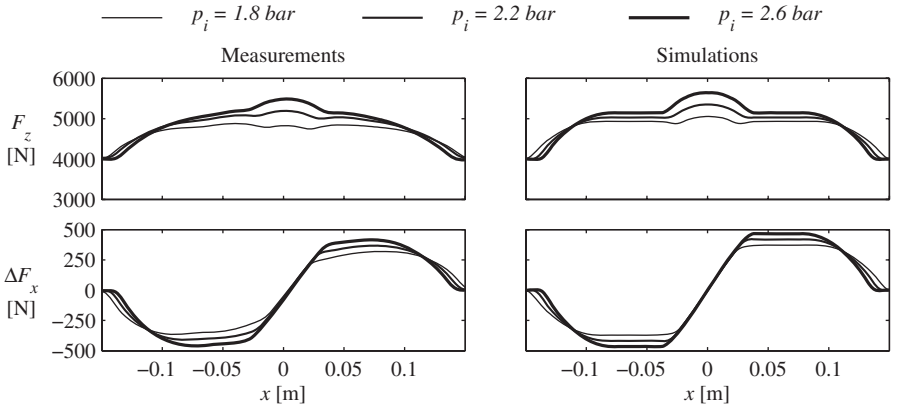

Figure 8. Low speed enveloping with fixed axle height (10 × 50 mm cleat).

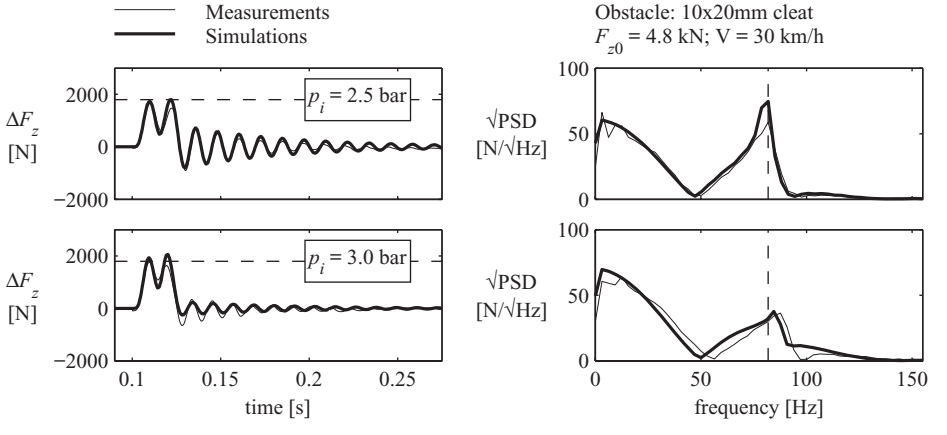

Figure 9. Cleat test of a passenger car tyre at a higher forward velocity. The dashed lines indicate the maximum vertical force and resonance frequency at 2.5 bar inflation pressure.

It should be noted that in principle for the parameterisation no additional cleat tests are required for the different inflation pressures. The shape of the cams remains constant and the eigenfrequencies of the tyre belt are modified using an empirical formula. Only the stiffness and the contact length depend on the tyre inflation pressure.

6. Concluding remarks

This paper shows the steps taken to enhance the Magic Formula model and to integrate various developments into a single tyre simulation model, suitable for different tasks: vehicle handling, ride and calculation of suspension loads. Though certainly open issues exist and research will continue, it can be seen as another step forward to an accurate digital representation of the physical tyre. The tyre model described in this paper has already been implemented in various multi-body software packages and can also be obtained directly from TNO Automotive. In addition to the MF-Tyre/MF-Swift 6.1 tyre model, the software package MF-Tool 6.1 is available for parameter identification, for more information we refer to the TNO Delft-Tyre website [11].

References

[1] H.B. Pacejka, *Tyre and Vehicle Dynamics*, 2nd ed., Butterworth-Heinemann, Oxford, UK, 2006, ISBN-13: 980-0-7506-6918-4.
[2] TNO, *MF-Tyre User Manual Version 5.2*, 2001
[3] E.J.H. de Vries, *Motorcycle Tyre Measurements and Models*, Proceedings of the 15th symposium Dynamics of Vehicles on Road and Tracks, IAVSD, Budapest, August 1997.
[4] J.J.M. van Oosten, C. Savi, M. Augustin, O. Bouhet, J. Sommer, and J.P. Colinot, *TiMe, TIre MEasurements forces and moments: a new standard for steady state cornering tire testing*, EAEC Conference, Barcelona, 30 June to 2 July, 1999.
[5] J.J.M. van Oosten, E. Kuiper, G. Leister, D. Bode, H. Schindler, J. Tischleder, and S. Kohne, *A new tyre model for TIME measurement data*, Tire Technology Expo 2003, Hannover, Germany, 2003.
[6] A.J.C. Schmeitz, I.J.M. Besselink, J. de Hoogh, and H. Nijmeijer, *Extending the magic formula and SWIFT tyre models for inflation pressure changes*, Reifen, Fahrwerk, Fahrbahn – VDI Conference, Hannover, Germany, 2005, pp. 201–225.
[7] I.B.A. op het Veld, *Enhancing the MF-Swift tyre model for inflation pressure changes*, DCT Rep. 2007.144, Eindhoven University of Technology, 2007.
[8] TNO, *Measurement requirements and TYDEX file generation for MF-Tyre/MF-Swift 6.1*. Available at www.delft-tyre.nl
[9] Michelin, *The Tyre – Rolling Resistance and Fuel Savings*, Société de Technologie Michelin-Ferrand, France, 2003, p. 84.
[10] A.J.C. Schmeitz, *A semi-empirical three-dimensional model of the pneumatic tyre rolling over arbitrarily uneven road surfaces*, Dissertation, Delft University of Technology, The Netherlands, 2004.
[11] TNO Delft-Tyre website. Available at www.delft-tyre.nl

Appendix. TNO MF-TYRE 6.1 Magic Formula equations

The Magic Formula can be considered as a nonlinear function with multiple inputs and outputs, as is shown in Figure A1. The model parameters, typically starting with the character p, q, r or s, are determined in a numerical optimisation process minimising the difference between the output of the Magic Formula and the measured forces and moments. In this process, the scaling coefficients, starting with the character λ, will remain equal to one. Please note that the difference between α_F and α_M disappears when the additional transient behaviour of the self-aligning moment is not taken into account, so $\alpha = \alpha_F = \alpha_M$.

When the inputs are far outside the measurement range (e.g. extremely high vertical loads or very large inclination angles), the extrapolation capabilities of the model can possibly fail. To prevent this from happening, the inputs to the Magic Formula are bounded and the Magic Formula is not evaluated outside this range, so

$$\kappa_{\min} < \kappa < \kappa_{\max}, \tag{A1}$$

$$\alpha_{\min} < \alpha_F < \alpha_{\max} \text{ and } \alpha_{\min} < \alpha_M < \alpha_{\max}, \tag{A2}$$

$$\gamma_{\min} < \gamma < \gamma_{\max}, \tag{A3}$$

$$p_{i,\min} < p_i < p_{i,\max}. \tag{A4}$$

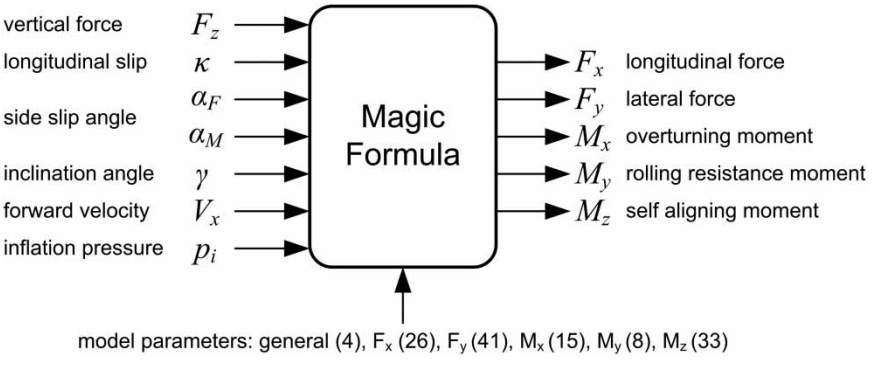

Figure A1. Inputs and outputs of the Magic Formula.

For the vertical force a range is also defined. When the vertical force F_z is outside this range, the Magic Formula is evaluated for the corresponding boundary ($F_{z,\min}$ or $F_{z,\max}$) when the vertical forces is below $F_{z,\min}$ the resulting forces and moments are scaled with the actual value of the vertical force. A simple example, if the vertical force equals 0.5 times $F_{z,\min}$, then the Magic Formula is evaluated for $F_{z,\min}$ and the resulting forces/moments are multiplied with a factor 0.5. No scaling is applied when the vertical force exceeds forces.

To make the Magic Formula equations dimensionless, the following parameters are introduced:

- unscaled free tyre radius of the non-rolling tyre R_0;
- nominal vertical force F_{z0};
- reference forward velocity V_0;
- nominal tyre inflation pressure p_{i0}.

To account for changes in the vertical force and tyre inflation pressure, dimensionless increments are introduced:

$$\mathrm{df}_z = \frac{F_z - F_{z0}}{F_z}, \tag{A5}$$

$$\mathrm{dp}_i = \frac{p_i - p_{i0}}{p_{i0}}. \tag{A6}$$

Many parameters of the MF-Tyre 6.1 tyre model are unchanged and have the same name as in the MF-Tyre 5.2 model. The additional parameter FITTYP has been introduced by TNO to uniquely identify equations. When FITTYP equals 61, we are dealing with a MF-Tyre 6.1 dataset.

Al *Longitudinal force F_x*

$$F_x = (D_x \sin[C_x \arctan\{B_x\kappa_x - E_x(B_x\kappa_x - \arctan(B_x\kappa_x))\}] + S_{Vx})G_{x\alpha}. \tag{A7}$$

A1.1 *Pure slip*

$$\kappa_x = \kappa + S_{Hx}, \tag{A8}$$

$$C_x = p_{Cx1}\lambda_{Cx}, \tag{A9}$$

$$D_x = \mu_x F_z, \tag{A10}$$

$$\mu_x = (p_{Dx1} + p_{Dx2}\,\mathrm{df}_z)\left(1 - p_{Dx3}\gamma^2\right)\left(1 + p_{px3}\,\mathrm{dp}_i + p_{px4}\,\mathrm{dp}_i^2\right)\lambda_{\mu x}, \tag{A11}$$

$$E_x = \left(p_{Ex1} + p_{Ex2}\,\mathrm{df}_z + p_{Ex3}\,\mathrm{df}_z^2\right)(1 - p_{Ex4}\,sgn\,(\kappa_x))\,\lambda_{Ex}, \tag{A12}$$

$$K_{x\kappa} = (p_{Kx1} + p_{Kx2}\,\mathrm{df}_z)\exp\left(p_{Kx3}\,\mathrm{df}_z\right)\left(1 + p_{px1}\,\mathrm{dp}_i + p_{px2}\,\mathrm{dp}_i^2\right)F_z\lambda_{Kx\kappa}, \tag{A13}$$

$$B_x = \frac{K_{x\kappa}}{C_x D_x}, \tag{A14}$$

$$S_{Hx} = (p_{Hx1} + p_{Hx2}\,\mathrm{df}_z)\lambda_{Hx}, \tag{A15}$$

$$S_{Vx} = (p_{Vx1} + p_{Vx2}\,\mathrm{df}_z)F_z\lambda_{Vx}\lambda_{\mu x}. \tag{A16}$$

A1.2 *Combined slip*

$$G_{x\alpha} = \frac{\cos[C_{x\alpha} \arctan\{B_{x\alpha}\alpha_s - E_{x\alpha}(B_{x\alpha}\alpha_s - \arctan(B_{x\alpha}\alpha_s))\}]}{\cos[C_{x\alpha} \arctan\{B_{x\alpha}S_{Hx\alpha} - E_{x\alpha}(B_{x\alpha}S_{Hx\alpha} - \arctan(B_{x\alpha}S_{Hx\alpha}))\}]}, \tag{A17}$$

$$\alpha_\mathrm{s} = \alpha_\mathrm{F} + S_{Hx\alpha}, \tag{A18}$$

$$B_{x\alpha} = (r_{Bx1} + r_{Bx3}\gamma^2)\cos\{\arctan[r_{Bx2}\kappa]\}\lambda_{xa}, \tag{A19}$$

$$C_{x\alpha} = r_{Cx1}, \tag{A20}$$

$$E_{x\alpha} = r_{Ex1} + r_{Ex2}\,\mathrm{df}_z, \tag{A21}$$

$$S_{Hx\alpha} = r_{Hx1}. \tag{A22}$$

When combined slip is not used, $G_{x\alpha} = 1$.

A2 *Lateral force F_y (input α_F)*

$$F_y = G_{y\kappa} F_{yp} + S_{Vy\kappa}. \tag{A23}$$

A2.1 *Pure slip*

$$F_{yp} = D_y \sin\left[C_y \arctan\left\{B_y\alpha_y - E_y\left(B_y\alpha_y - \arctan\left(B_y\alpha_y\right)\right)\right\}\right] + S_{Vy}, \tag{A24}$$

$$\alpha_y = \alpha_{\mathrm{F}} + S_{Hy}, \tag{A25}$$

$$C_y = p_{Cy1}\lambda_{Cy}, \tag{A26}$$

$$D_y = \mu_y F_z, \tag{A27}$$

$$\mu_y = \left(p_{Dy1} + p_{Dy2}\,\mathrm{df}_z\right)\left(1 - p_{Dy3}\gamma^2\right)\left(1 + p_{py3}\,\mathrm{dp}_i + p_{py4}\,\mathrm{dp}_i^2\right)\lambda_{\mu y}, \tag{A28}$$

$$E_y = \left(p_{Ey1} + p_{Ey2}\,\mathrm{df}_z\right)\left(1 + p_{Ey5}\gamma^2 - \left(p_{Ey3} + p_{Ey4}\gamma\right)\mathrm{sgn}\left(\alpha_y\right)\right)\lambda_{Ey}, \tag{A29}$$

$$K_{y\alpha} = p_{Ky1}F_{z0}\left(1 + p_{py1}\,\mathrm{dp}_i\right)\sin\left[p_{Ky4}\arctan\left\{\frac{F_z}{\left(p_{Ky2} + p_{Ky5}\gamma^2\right)\left(1 + p_{py2}\,\mathrm{dp}_i\right)F_{z0}}\right\}\right]\left(1 - p_{Ky3}\,|\gamma|\right)\lambda_{Ky\alpha}, \tag{A30}$$

$$K_{y\gamma} = \left(p_{Ky6} + p_{Ky7}\,\mathrm{df}_z\right)\left(1 + p_{py5}\,\mathrm{dp}_i\right)F_z\lambda_{Ky\gamma}, \tag{A31}$$

$$B_y = \frac{K_{y\alpha}}{C_y D_y}, \tag{A32}$$

$$S_{Hy} = S_{Hy0} + S_{Hy\gamma}, \tag{A33}$$

$$S_{Hy0} = \left(p_{Hy1} + p_{Hy2}\,\mathrm{df}_z\right)\lambda_{Hy}, \tag{A34}$$

$$S_{Hy\gamma} = \frac{K_{y\gamma}\gamma - S_{Vy\gamma}}{K_{y\alpha}}, \tag{A35}$$

$$S_{Vy} = S_{Vy0} + S_{Vy\gamma}, \tag{A36}$$

$$S_{Vy0} = F_z\left(p_{Vy1} + p_{Vy2}\,\mathrm{df}_z\right)\lambda_{Vy}\lambda_{\mu y}, \tag{A37}$$

$$S_{Vy\gamma} = F_z\left(p_{Vy3} + p_{Vy4}\,\mathrm{df}_z\right)\gamma\,\lambda_{Ky\gamma}\lambda_{\mu y}. \tag{A38}$$

A2.2 *Combined slip*

$$S_{Vy\kappa} = D_{Vy\kappa}\,\sin\left(r_{Vy5}\,\arctan\left(r_{Vy6}\kappa\right)\right)\lambda_{Vy\kappa}, \tag{A39}$$

$$D_{Vy\kappa} = \mu_y F_z\left(r_{Vy1} + r_{Vy2}\,\mathrm{df}_z + r_{Vy3}\gamma\right)\cos\left(\arctan\left(r_{Vy4}\alpha_F\right)\right), \tag{A40}$$

$$G_{y\kappa} = \frac{\cos\left[C_{y\kappa}\,\arctan\left\{B_{y\kappa}\kappa_{\mathrm{s}} - E_{y\kappa}\left(B_{y\kappa}\kappa_{\mathrm{s}} - \arctan\left(B_{y\kappa}\kappa_{\mathrm{s}}\right)\right)\right\}\right]}{\cos\left[C_{y\kappa}\,\arctan\left\{B_{y\kappa}S_{Hy\kappa} - E_{y\kappa}\left(B_{y\kappa}S_{Hy\kappa} - \arctan\left(B_{y\kappa}S_{Hy\kappa}\right)\right)\right\}\right]}, \tag{A41}$$

$$\kappa_{\mathrm{s}} = \kappa + S_{Hy\kappa}, \tag{A42}$$

$$B_{y\kappa} = \left(r_{By1} + r_{By4}\gamma^2\right)\cos\{\arctan[r_{By2}(\alpha_f - r_{By3})]\}\lambda_{y\kappa}, \tag{A43}$$

$$C_{y\kappa} = r_{Cy1}, \tag{A44}$$

$$E_{y\kappa} = r_{Ey1} + r_{Ey2}\,\mathrm{df}_z, \tag{A45}$$

$$S_{Hy\kappa} = r_{Hy1} + r_{Hy2}\,\mathrm{df}_z. \tag{A46}$$

A3 *Overturning moment M_x*

$$\begin{aligned} M_x = R_0 F_z \lambda_{Mx}\Bigg\{ & q_{sx1}\lambda_{VMx} - q_{sx2}\gamma\left(1 + p_{pmx1}\,\mathrm{dp}_i\right) + q_{sx3}\frac{F_y}{F_{z0}} \\ & + q_{sx4}\,\cos\left[q_{sx5}\,\arctan\left(\left(q_{sx6}\frac{F_z}{F_{z0}}\right)^2\right)\right]\cdot\sin\left[q_{sx7}\gamma + q_{sx8}\,\arctan\left(q_{sx9}\frac{F_y}{F_{z0}}\right)\right] \\ & + q_{sx10}\,\arctan\left(q_{sx11}\frac{F_z}{F_{z0}}\right)\gamma\Bigg\}. \end{aligned} \tag{A47}$$

A4 *Rolling resistance moment M_y*

$$M_y = -R_0 F_{z0} \lambda_{My} \left(q_{sy1} + q_{sy2} \frac{F_x}{F_{z0}} + q_{sy3} \left| \frac{V_x}{V_0} \right| + q_{sy4} \left(\frac{V_x}{V_0} \right)^4 + q_{sy5} \gamma^2 + q_{sy6} \frac{F_z}{F_{z0}} \gamma^2 \right) \cdot \left(\frac{F_z}{F_{z0}} \right)^{q_{sy7}} \left(\frac{p}{p_0} \right)^{q_{sy8}} \tag{A48}$$

When combined slip is not used, $S_{Vy\kappa} = 0$ and $G_{y\kappa} = 1$.

A5 *Self-aligning moment M_z (input α_M)*

$$M_z = -t F_{yp0} G_{y\kappa 0} + M_{zr} + s F_x, \tag{A49}$$

where $F_{yp0} G_{y\kappa 0}$ is the combined slip side force with zero inclination angle ($\gamma = 0$).

$$\alpha_t = \alpha_M + S_{Ht}, \tag{A50}$$

$$S_{Ht} = q_{Hz1} + q_{Hz2}\, df_z + (q_{Hz3} + q_{Hz4}\, df_z)\, \gamma, \tag{A51}$$

$$\alpha_r = \alpha_M + S_{Hy} + \frac{S_{Vy}}{K_{y\alpha}}, \tag{A52}$$

A5.1 *Pure slip*

$$\alpha_{t,eq} = \alpha_t, \quad \alpha_{r,eq} = \alpha_r, \quad s = 0. \tag{A53}$$

A5.2 *Combined slip*

$$\alpha_{t,eq} = \arctan \sqrt{\tan^2(\alpha_t) + \left(\frac{K_{x\kappa}}{K_{y\alpha}} \right)^2 \kappa^2} \cdot \mathrm{sgn}(\alpha_t), \tag{A54}$$

$$\alpha_{r,eq} = \arctan \sqrt{\tan^2(\alpha_r) + \left(\frac{K_{x\kappa}}{K_{y\alpha}} \right)^2 \kappa^2} \cdot \mathrm{sgn}(\alpha_r), \tag{A55}$$

$$s = \left(s_{sz1} + s_{sz2} \left(\frac{F_y}{F_{z0}} \right) + (s_{sz3} + s_{sz4}\, df_z)\, \gamma \right) R_0 \lambda_s, \tag{A56}$$

A5.3 *Pneumatic trail t*

$$t = D_t \cos\left[C_t \arctan\left\{ B_t \alpha_{t,eq} - E_t \left(B_t \alpha_{t,eq} - \arctan\left(B_t \alpha_{t,eq} \right) \right) \right\} \right] \cos(\alpha_M), \tag{A57}$$

$$B_t = \left(q_{Bz1} + q_{Bz2}\, df_z + q_{bz3}\, df_z^2 \right) \left(1 + q_{Bz4} \gamma + q_{Bz5} |\gamma| \right) \frac{\lambda_{Ky\alpha}}{\lambda_{\mu y}}, \tag{A58}$$

$$C_t = q_{Cz1}, \tag{A59}$$

$$D_t = (q_{Dz1} + q_{Dz2}\, df_z) \left(1 - p_{pz1}\, dp_i \right) \left(1 + q_{Dz3} \gamma + q_{Dz4} \gamma^2 \right) F_z \frac{R_0}{F_{z0}} \lambda_t, \tag{A60}$$

$$E_t = \left(q_{Ez1} + q_{Ez2}\, df_z + q_{Ez3}\, df_z^2 \right) \left(1 + (q_{Ez4} + q_{Ez5} \gamma) \left(\frac{2}{\pi} \right) \arctan\left(B_t C_t \alpha_t \right) \right). \tag{A61}$$

A5.4 *Residual moment M_{zr}*

$$M_{zr} = D_r \cos[\arctan(B_r \alpha_{r,\mathrm{eq}})] \cos(\alpha_{\mathrm{M}}), \tag{A62}$$

$$B_r = q_{Bz9} \frac{\lambda_{Ky\alpha}}{\lambda_{\mu y}} + q_{Bz10} B_y C_y, \tag{A63}$$

$$D_r = \begin{bmatrix} (q_{Dz6} + q_{Dz7}\,\mathrm{df}_z)\lambda_r + (q_{Dz8} + q_{Dz9}\,\mathrm{df}_z)(1 + p_{pz2}\,\mathrm{dp}_i)\gamma\,\lambda_{Kz\gamma} \\ +(q_{Dz10} + q_{Dz11}\,\mathrm{df}_z)\gamma|\gamma|\lambda_{Kz\gamma} \end{bmatrix} F_z R_0 \lambda_{\mu y}. \tag{A64}$$